Elastic-displacement field of an isolated surface step

John Stewart, Oliver Pohland, and J. Murray Gibson
Loomis Laboratory of Physics, University of Illinois at Urbana-Champaign, 1110 West Green Street, Urbana, Illinois 61801-3080
(Received 6 October 1993; revised manuscript received 10 January 1994)

The asymptotic elastic-displacement field of a surface step is shown to result from a planar force distribution which is composed of two point elastic dipoles, one oriented along the surface of arbitrary magnitude and one normal to the surface with dipole moment ag where a is the step height and g is the surface stress. The analytic form of the dipole displacement field for an isotropic material is presented. Experimental and simulated TEM images of the asymptotic displacement field are presented which demonstrate the dipolar nature of the force distribution. The normal dipole moment of a monatomic step on Si(111)(7×7) is computed to be 0.58±0.04 eV/Å. The tangential dipole moment is measured to be 1.46±0.3 eV/Å. The stress and strain tensors for an isolated step and the displacement field for a stepped surface are presented.

I. INTRODUCTION

Recent advances in transmission electron microscopy (TEM) allow the imaging of the elastic-displacement field of crystalline surface features such as adatoms, steps, and phase boundaries.[1,2] The techniques represent a challenge to the theory of the elastic field of surface features, since they allow quantitative information about the multipole moments to be extracted, if the form of the asymptotic displacement field can be supplied.

The elastic field of a step is the central quantity in understanding interactions of surface features. A surface step exerts force on the bulk crystal which causes the crystal to deform. The deformations are described by the elastic-displacement field. If the undeformed location of an atom is $\mathbf{r}$ and the location after deformation is $\mathbf{r}'$, then the displacement field $\mathbf{u}$, the distance the atom at $\mathbf{r}$ is displaced, is defined by $\mathbf{r}'=\mathbf{r}+\mathbf{u}(\mathbf{r})$. Steps interact through their displacement fields and the energy of this interaction contributes to the surface free-energy density and thus affects the equilibrium crystal shape. Steps also interact elastically with surface diffusers and vacancies. Field-ion-microscope (FIM) experiments observe an attraction between an adatom on the terrace above the step and the step edge.[3] The interaction of a step and an adatom on the lower terrace should be very much like the interaction between adatoms and a large cluster. FIM experiments observe an exclusion zone devoid of diffusers of width 10 Å surrounding a cluster.[4] Adatoms also interact elastically[5] with each other leading to an interaction energy with a complicated angular dependence.[6] An understanding of the step displacement field is essential to advancing surface theory beyond fixed lattice models.

The purpose of this work is to present a clear and careful analysis of the asymptotic displacement field of a surface step, to understand approximations made by previous works, and to present exact results when possible. In Sec. II, the elastic multipole expansion is developed to allow the extraction of the asymptotic field from an arbitrary force distribution. The form of the displacement field of a step and the elastic multipole moments are computed. In Sec. III, the analytic form of the surface Green's function and the dipole displacement fields are given for an isotropic elastic material. In Sec. IV, the dipole fields are quantitatively tested against a simple computational model of a step. In Sec. V, the effect of cubic anisotropy is evaluated. Section VI presents TEM images that determine the leading multipole moment of a step. The theoretical displacement field is used to extract a quantitative value for the leading multipole moment of a monatomic step on Si(111)(7×7). The stress and strains tensors for a surface dipole and the displacement field of a uniformly stepped surface are reported in the Appendix.

II. GENERAL RESULTS

The usual approach to the problem of step elasticity is to approximate the force distribution at a step by a force distribution projected on a flat interface and then use isotropic linear elasticity theory to compute the displacement field.[7,8] This involves both an approximation to the force distribution and the approximation of using an isotropic theory to model a crystalline system. In this section, the projection of the force on a plane is investigated. The general form of the elastic multipole expansion is presented and used to derive exact results about the leading multipole moments.

A. Elastic multipole expansion

Figure 1(a) shows a cross section of a straight step infinite in the y direction. The elastic problem of an infinite straight step reduces to a two-dimensional problem with both the force distribution and the elastic-displacement field independent of y. The mathematical tools available for computing the displacement field work only for flat surfaces, so the stepped surface must be replaced by a mechanically equivalent flat surface. For the isolated step, the natural flat surface is the plane AB in Fig. 1(a). The correct force distribution on the plane AB, $f^{AB}(x)$ is found by separating the crystal along the plane, thus removing the atoms forming the step and replacing

them with the force they exert on the plane AB. The separated crystal is shown in Fig. 1(b). The removed portions above AB will be called the step system. This does not involve an approximation because it is always possible to separate an extended body and replace the removed portions by the forces they exert. Also, any surface forces acting on the atoms in plane AB are treated as external forces and absorbed into f^{AB}. This procedure converts the complicated problem of a stepped surface acted on by surface stresses into the problem of a bulk crystal acted on by an external force distribution at its flat surface. The procedure does not introduce any approximations, since f^{AB} is simply the physical force distribution on the plane AB. It is the displacement field generated by this force distribution that is observed experimentally. Two sets of forces contribute to f^{AB} for an isolated step, a localized force distribution at the step, the forces f_s in Fig. 1(b), and the forces exerted by the unbalanced surface stresses at the edges of the crystal.

The force distribution f^{AB} has no simple relationship to the microscopic forces on the surface atoms. It contains the response forces generated by the excess stiffness

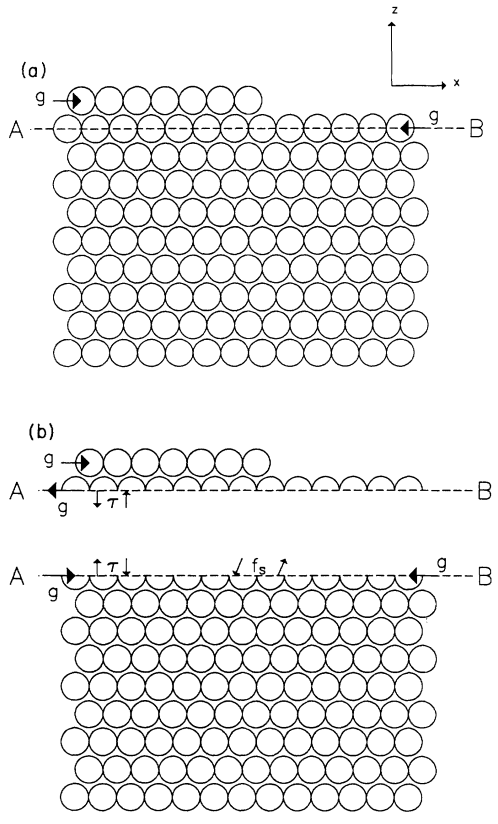

FIG. 1. (a) Cross section of an infinite straight step. The vector **g** is the force exerted by the unbalanced surface stress at the edge of the crystal. (b) Separation of the crystal that allows the computation of the elastic-displacement fields. The torque τ is generated by the force exerted by the unbalanced surface stress. The separation of the crystal does not require splitting the individual atoms, but induced surface forces and long-range forces from the step are included in the step system, so the force distribution f^{AB} does not vanish to the right of the step.

of the surface and the elastic forces generated by straining the layer of atoms forming the step. The step system filters the force distribution on its surface as those forces are communicated across the plane AB. Therefore, any attempt to use information extracted from f^{AB} to model the local microscopic force distribution is uncontrolled. Equally dangerous is proposing a microscopic distribution of forces on the physical surface and computing f^{AB}, since an accurate calculation would include a self-consistent treatment of the force distribution generated by excess surface stiffness and the mechanical properties of the extra row of atoms forming the step.

The planar force distribution f^{AB} allows the computation of the displacement field of the material below the plane AB as the convolution of f^{AB} with the relevant Green's function:

$$u_i(x,z)=\int_L dx' G_{ij}(x-x',z) f_j^{AB}(x') , \tag{2.1}$$

where i and j are either x or z, repeated indices are summed, u_i is the component of the displacement field, and G_{ij} is the four component tensor Green's function. The x axis coincides with the AB plane and the origin will be set to the center of force. The Green's function G_{ij} is the solution to the problem of a line force f_i at the origin, with the displacement field given by $u_i=G_{ij}f_j$. For now, the Green's function is left arbitrary. Its form depends on the symmetries of the bulk crystal. The force distribution from the step is assumed local and contained in the region L. We seek a solution for the displacement field outside this region but far from the boundaries of the crystal, so the forces from the surface stress at the edge of the crystal are excluded from the integration. The asymptotic field of a localized disturbance is found by performing a multipole expansion. Since the region L is finite and in reality small, it makes sense to expand the Green's function in a Taylor's series:

$$G_{ij}(x-x',z)=\sum_n \frac{(-1)^n (x')^n}{n!} \frac{\partial^n G_{ij}(x,z)}{\partial x^n} . \tag{2.2}$$

Define the multipole Green's functions

$$D_{ij}^n(x,z)=\frac{(-1)^n}{n!} \frac{\partial^n G_{ij}(x,z)}{\partial x^n} \tag{2.3}$$

and the multipole moments

$$d_i^n=\int_L dx\, f_i^{AB}(x) x^n . \tag{2.4}$$

Substituting the Taylor expansion and using these definitions, (2.1) can be rewritten as

$$u_i(x,z)=\sum_n D_{ij}^n(x,z) d_j^n . \tag{2.5}$$

The utility of this expression is that displacement fields of higher-order multipoles decay more rapidly than those of lower-order multipoles. For an isotropic solid, $D^0 \sim \log(r)$ and $D^n \sim 1/r^n$ where $r=\sqrt{x^2+z^2}$. Therefore, the asymptotic field is given by the lowest-order multipole field allowed by the constraints of the problem. The multipole expansion was first applied to surface elas-

tic problems by Marchenko and Parshin.[8] Recently, the multipole expansion has been used to characterize the interactions of various surface features.[7] In the next section, mechanical constraints are used to compute the lowest-order multipole moments.

B. Mechanical constraints

To generate the planar force distribution, the stepped crystal is separated into two pieces, the row of atoms forming the step, called the step system, and rest of the crystal. Each piece must be in mechanical equilibrium. For the bulk crystal to be in mechanical equilibrium, there can be no net force or torque applied by the forces f^{AB}, therefore,

$$\int_{AB} dx\, f_i^{AB}(x) = \int_L dx\, f_i^{AB}(x) + \int_{\text{rest}} dx\, f_i^{AB}(x) = 0 \tag{2.6}$$

and

$$\int_{AB} dx\, (\mathbf{r}\times\mathbf{f}^{AB}) = \int_L dx\, (\mathbf{r}\times\mathbf{f}^{AB}) + \int_{\text{rest}} dx\, (\mathbf{r}\times\mathbf{f}^{AB}) = 0\ . \tag{2.7}$$

In each case, the full integral over the plane has been separated into an integral over the step force distribution and an integral over the rest of the plane. The integrals over the rest of the plane contain the forces from the surface stress $\mathbf{g}$ at the edge of the crystal and the torques τ they generate, Fig. 1(b). The step system must, also, be in mechanical equilibrium. It is acted on by a force $\mathbf{g}$ at its left side, which generates a torque about a point in the plane AB directly below the left edge of the crystal, $\tau = ag\hat{\mathbf{y}}$ where $\hat{\mathbf{y}}$ is the unit vector in the y direction directed into the page and g is the magnitude of $\mathbf{g}$. The forces and torques on the step system from the surface stress must be balanced by forces applied across the plane AB by the rest of the crystal. The step communicates a force $g\hat{\mathbf{x}}$ and a torque $\tau = ag\hat{\mathbf{y}}$ to the plane AB, shown in Fig. 1(b). It is assumed the edge of the crystal is sufficiently separated from the step force distribution so they can be treated independently. The force communicated by the step is balanced by the surface stress at the opposite edge of the crystal and the integral of the force over the rest of the crystal vanishes. The force conservation law, (2.6), then gives

$$\int_L dx\, f_i^{AB}(x) = d_i^0 = 0\ . \tag{2.8}$$

The torque integral over the rest of the surface gives the value $ag\hat{\mathbf{y}}$, the value from the step, because the surface stresses at the right of the AB plane are directed along the plane and do not contribute. The torque balance, (2.7), becomes

$$\int_L dx\, (\mathbf{r}\times\mathbf{f}^{AB}) = -\int_L dx\, x f_z^{AB}(x)\hat{\mathbf{y}} = -d_z^1\hat{\mathbf{y}} = -ag\hat{\mathbf{y}}\ . \tag{2.9}$$

Application of mechanical constraints allows the computation of three of the multipole moments: $d_x^0 = d_z^0 = 0$ and $d_z^1 = ag$. Note, the value of the z dipole is for a down step as shown in Fig. 1(a), the moment changes sign for an up step. These are exact results for the force distribution f^{AB}, not simply results for the microscopic surface force distribution, which must then be projected upon the flat plane in an uncontrolled manner to compute the displacement field. The z-dipole moment result was stated previously by Marchenko and Parshin[8] and Nozières[9] for the full surface force distribution. The contribution of the above analysis is to show the z-dipole moment is ag without approximation for the observed force distribution f^{AB}, that it survives the projection process, and that the projection process does not expose fictitious monopoles. Note that this result is somewhat unexpected because simple, and incorrect, projections for the full surface force like parallel transport of the force vectors do not preserve the z-dipole moment. We also note that it is difficult to connect the full surface force distribution with the distribution on the plane even perturbatively because the step involves a single layer of atoms. For the experimental analysis that follows, it is vital to be able to fix one of the dipoles so that the other can be extracted from the data. The existence of a dipole moment d_z^1 shows that the asymptotic displacement field will be a dipole field.

The separation discussed above involves applying mechanics on the length scale of atomic distances, since for a monatomic step the step system contains only a single layer of atoms. It is, therefore, necessary to take extreme care in the taking of limits and of coarse-graining to avoid quantum effects. A more detailed discussion of the separation process follows. The elastic-displacement field involves the long time average of the center of mass of the atoms in the crystal. A microscopic representation of the time-averaged force on the atoms must be developed. Introduce R_t the location of the center of mass of an atom averaged over time t. The wave function associated with this variable $\psi(R_t)$ is very well localized because of the time average and the localization of the atoms in the crystal lattice. If $V(R_t)$ is the effective potential energy of interaction between the atoms, then Ehrenfest's theorem allows the definition of a force $F = \langle \nabla V(R_t)\rangle = d^2\langle R_t\rangle/dt^2$, where $\langle\ \rangle$ takes the expectation value. Since the time-averaged center of mass is well localized, this force will behave classically. In this manner, a force distribution between the single atomic layer of the step system and the bulk crystal is constructed. This force distribution includes forces between the step system and the atoms in plane AB and longer-range forces between the step system and atoms deeper in the bulk. The forces between the step system and the atoms in the plane AB are surface forces, but the longer-ranged forces are body forces that must be reduced to surface forces to construct f^{AB}. The total distribution must balance the torque ag applied by the surface stresses at infinity. Note, it does not matter how the surface stress is distributed perpendicular to the surface, there is always ag torque to be balanced by the step. Since we wish to observe the same asymptotic displacement field with surface forces replacing the longer-range body forces, the surface force distribution, which replaces the body forces, must have the same torque as the body force distribution. Therefore, the effective surface force distribution from

the step system has the same torque as the surface plus body force distribution, ag. Finally, absorb any remaining surface forces from the elastic surface response or any other source into the surface force distribution. Since these forces are torque free, this does not change the torque from ag. In this way, the surface force distribution f^{AB} is constructed by separating the crystal. The resulting force distribution f^{AB} varies over extremely short length scales. The computation of the dipole moment effectively coarse grains the force distribution over the entire crystal surface.

III. ISOTROPIC RESULTS

The results of the previous section were derived without specifying the form of G. In this section, G is given for an isotropic material and the dipole displacement tensor D^1 is calculated. The displacement field for an infinite line force on the surface of an isotropic material is a textbook problem in elasticity theory.[10] For an isotropic material G has the form

$$\begin{aligned}
G_{xx}&=\frac{1}{\pi E_2}\left[-2\ln(r)-(1+\nu_2)\frac{z^2}{r^2}\right],\\
G_{zx}&=\frac{1}{\pi E_2}\left[-(1-\nu_2)\sin^{-1}\left(\frac{x}{r}\right)+(1+\nu_2)\frac{xz}{r^2}\right],\\
G_{xz}&=\frac{1}{\pi E_2}\left[(1-\nu_2)\sin^{-1}\left(\frac{x}{r}\right)+(1+\nu_2)\frac{xz}{r^2}\right],\\
G_{zz}&=\frac{1}{\pi E_2}\left[-2\ln(r)-(1+\nu_2)\frac{x^2}{r^2}\right],
\end{aligned}\tag{3.1}$$

where $r^2=x^2+z^2$. The constants E_2 and ν_2 are two-dimensional analogues to Young's modulus and Poisson's ratio. They are related to the more familiar three-dimensional expressions by $E_2=E/(1-\nu^2)$ and $\nu_2=\nu/(1-\nu)$, where E is Young's modulus and ν is Poisson's ratio. Constant terms are dropped from G because they depend on the choice of boundary conditions and vanish as higher-order multipoles are generated. This form of G assumes a state of plane strain. The tensor G is a combination of two displacement fields; $\mathbf{u}^x=(G_{xx},0,G_{zx})$ the displacement field of a unit positive x directed line force, and $\mathbf{u}^z=(G_{xz},0,G_{zz})$ the displacement field of a unit positive z directed line force. Each of these displacement fields individually satisfy the mechanical equilibrium condition for an isotropic linear elastic material:

$$\mu\nabla^2\mathbf{u}+(\lambda+\mu)\nabla(\nabla\cdot\mathbf{u})=0\ , \tag{3.2}$$

where λ and μ are the Lamé coefficients. The stress derived from $\mathbf{u}^x$ and $\mathbf{u}^z$, σ^x_{ij} and σ^z_{ij}, respectively, is singular at the origin as one would expect for an applied line force. The relation of the displacement field to the stress is discussed in the Appendix. The line force at the origin is found by integrating the stress over the surface of a cylindrical cavity of radius r and then taking the limit $r\to 0$. The force $\mathbf{F}$ that must be applied to the cavity to generate the displacement fields is found by evaluating

$$F_i=-\int_{-\pi/2}^{\pi/2}\sigma_{ij}r_j d\theta\ , \tag{3.3}$$

where r_i is the radial vector from the origin and θ is measured from the $-z$ axis. Performing (3.3) for σ^x gives $\mathbf{F}=(1,0,0)$ a unit x directed force monopole and for σ^z gives $\mathbf{F}=(0,0,1)$ a unit z directed force monopole. With the Green's function G the dipole displacement fields are constructed.

Applying (2.3) allows the computation of D^1 as

$$\begin{aligned}
D^1_{xx}&=\frac{2}{\pi E_2 r^4}[x^3-\nu_2 xz^2]\ ,\\
D^1_{zx}&=\frac{2}{\pi E_2 r^4}[-z^3+\nu_2 zx^2]\ ,\\
D^1_{xz}&=\frac{2}{\pi E_2 r^4}[zx^2-\nu_2 z^3]\ ,\\
D^1_{zz}&=\frac{2}{\pi E_2 r^4}[x^3+(2+\nu_2)xz^2]\ .
\end{aligned}\tag{3.4}$$

The asymptotic form of the displacement field $1/r$ and the order of the leading multipole as the dipole allows a closer examination of the assumption of localization and the validity of the multipole expansion for terms higher than the leading order. Since the surface displacement field decays as $1/r$, the strain at the surface and the induced surface stress from the step system and the surface elastic response decay as $1/r^2$, and, therefore, there is an induced surface force due to the surface elastic response which decays as $1/r^3$. This forces a more general definition of L as the length over which the leading-order multipole integral d^1 converges. Note that the long-range part of the dipole integral, $d^1_x=\int dx\, x(1/x^3)$, does converge and, therefore, the x-dipole moment does exist. However, due to this nonlocal force distribution the higher-order multipole moments do not exist since $\int dx\, x^n(1/x^3)\to\infty$ for $n>1$. Therefore, the asymptotic form of the displacement field cannot be systematically corrected by the addition of higher-order moments. Correction of the asymptotic dipole result involves evaluating the full integral (2.1). The expansion in (2.5) must be viewed as an asymptotic expansion that diverges after the first term. It is necessary then to verify that the divergent higher-order terms do not introduce corrections to the dipole fields which decay as $1/r$. The concern is that the divergent higher-order multipoles might renormalize the dipole moment from the value computed as the integral of f^{AB}. It is, therefore, necessary to explicitly verify that $u_i\to D^1_{ij}d^1_j$ as $r\to\infty$. We do this by numerically computing (2.1) at the surface for a surface force distribution which decays as $1/r^3$. Define $f^l_x=\mathrm{sgn}(x)/(1+x^2)^{3/2}\to 1/x^3$. The dipole moment of this force distribution is $d^1_x=\int dx\, xf^l_x=2$. The displacement field at the surface is

$$\begin{aligned}
u_x(x,0)&=\int G_{xx}f^l_x dx'\\
&=\frac{-1}{\pi E_2}\int\ln[(x-x')^2]f^l_x(x')dx'\ .
\end{aligned}\tag{3.5}$$

If there is no correction to the dipole fields coming from

the higher-order moments, then the displacement field at the surface should approach $u_x^d(x,0)=D_{xx}^1 d_x^1=2d_x^1/\pi E_2 x$. Numerical evaluation of the ratio $u_x(x,0)/u_x^d(x,0)$ converges to one demonstrating that the multipole expansion does correctly capture the leading-order multipole. Note that this is the result we would intuitively expect. Well outside the range of convergence of a dipolar force distribution, the displacement field should be dipolar with the dipole moment of the force distribution. In the future, we hope to extend this result and redefine the higher-order multipoles so the divergence is removed.

IV. COMPUTATIONAL TESTS

The above expression for D is the simplest possible for a surface step, a pure dipole field. Before using the dipole displacement field to extract the dipole moments from an experimental TEM image, the theoretical displacement fields are tested using a simple computational model.

Rather than use a physical model of a solid, such as a molecular-dynamics solid, which would allow only a qualitative test of the asymptotic step fields, a simplified two-dimensional solid is used so a quantitative test can be performed. The model used incorporates the basic physics of the problem: a discrete crystalline solid with an atomic step on a surface that experiences surface stress. Through suitable choices of the force parameters the model is made isotropic. Since the step problem, under the assumption of plane strain, reduces to a two-dimensional problem, the displacement fields apply to a two-dimensional solid. The computational model is a two-dimensional solid composed of masses and perfect linear springs. The unit cell for the crystal is a square of unit area with masses at each corner and a mass at the center. Springs are added along the edges of the square with spring constant k_1 and between the center mass and each corner with spring constant k_2. The resulting two-dimensional crystal is shown in Fig. 2. All springs are unstretched and have spring constant one. This choice for the geometry of the masses and the spring constants generates an isotropic two-dimensional crystal with $E_2=\frac{4}{3}$ and $\nu_2=\frac{1}{3}$. The unit cell is repeated to make a crystal with a step as shown in Fig. 2. Surface stress is added to the model by adding an extra set of springs, with spring constant k_3, between the surface atoms. These springs have equilibrium lengths shorter than the distance between the surface atoms. In the simulation presented, the surface springs have equilibrium length 0.95 and spring constant $k_3=0.1$. Since the step height is 0.5, the value of d_z^1 from (2.9) is 0.0025. The addition of extra springs to the surface gives it added stiffness, just as physical crystals have a surface elastic response. Also, the step does not step down a full bulk unit cell giving the step system unique elastic properties; another effect that exists in Si.

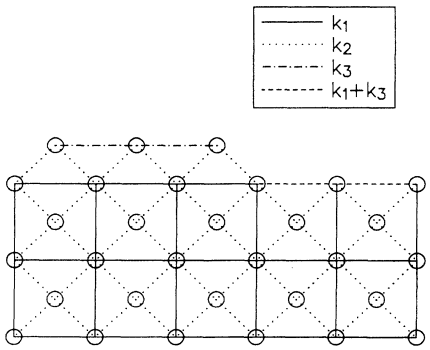

FIG. 2. Computational two-dimensional crystal. The lines represent the springs. The line k_1+k_3 represents the two springs with spring constants k_1 and k_3 between the same masses.

The crystal was annealed using a simple viscous dynamics to find the equilibrium displacement field. A 40×40 lattice was used with the top boundary free and the other sides adjusted to the theoretic displacements to eliminate the extreme finite-size effects inherent in surface force distributions. The annealed displacement field is shown as the vectors with open arrowheads in Fig. 3(a), with the circles being the undisplaced locations of the masses. The surface truncation is the same as in Fig. 2. The displacement field is scaled by $r=\sqrt{x^2+z^2+1}$ and a magnification factor to make the asymptotic displace-

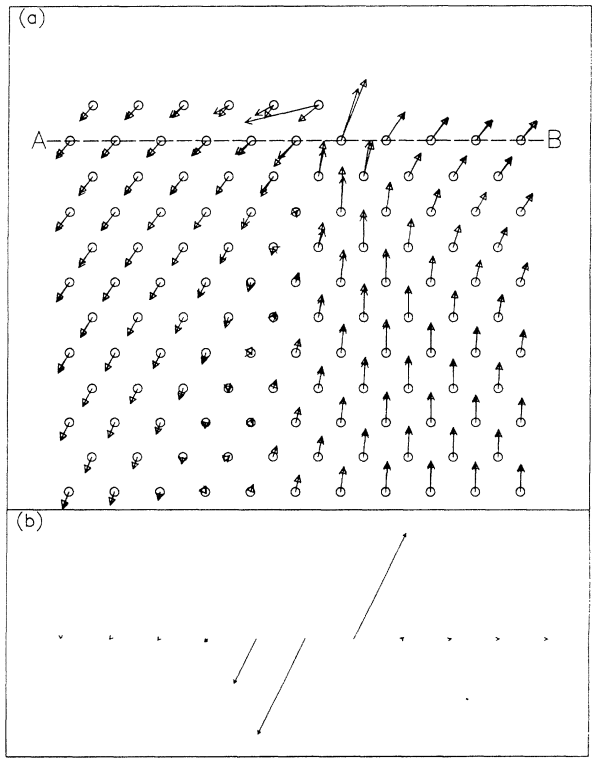

FIG. 3. Computational test of isotropic dipole fields: (a) Two-dimensional crystal. The circles represent the undeformed location of the masses. The open arrowheads are the displacement of the masses upon annealing the crystal multiplied by r and a magnification factor, where r is the distance from the step edge with a cutoff. The closed arrowheads are the calculated field using only the dipole moments. (b) Force distribution on plane AB. The two longest vectors have been reduced by a factor of 5 so the asymmetry generated by the step can be seen.

ment field visible. The origin of r is the center of force x_c defined as

$$x_c=\frac{1}{2}\left[\frac{\int_L dx\, x\,(f_x^{AB})^2}{\int_L dx\,(f_x^{AB})^2}+\frac{\int_L dx\, x\,(f_z^{AB})^2}{\int_L dx\,(f_z^{AB})^2}\right]. \quad (4)$$

Although nothing in the analysis forces this choice for the origin, the closer the origin is to the force center the better the approximation of the multipole expansion. The force distribution f^{AB} can be measured computationally and the force center lies under the step edge. With this choice of the origin the dipole moments can be measured giving $d_x^1=0.002\,87$ and $d_z^1=0.002\,486$. The z-dipole moment is extremely close to our theoretic value 0.0025, thus showing the validity of using ag as the step moment. The value of the x dipole could be arbitrarily changed by adding extra springs between the step layer and the AB layer. The extra springs model relaxations at the step edge. It was impossible to affect the z-dipole moment by any local force distribution at the step, thus showing that $d_z^1=ag$ is a general result. Using the measured x-dipole moment and the theoretical z-dipole moment, the dipole displacement field is calculated and shown as the closed arrowhead vector field in Fig. 3(a). The agreement for masses within the bulk crystal is excellent. There are no free parameters in the theoretical displacement field since d_x^1 is measured and d_z^1, E_2, and ν_2 are calculated. The displacement field for the step system is computed by evaluating the calculated fields at $z=+0.5$.

There are two regions where the agreement between the annealed and calculated fields is not perfect, in the step system and in the bulk crystal near the center of force. To test what part of this error is the result of keeping only the lowest-order multipole, the displacement field was computed by numerically evaluating (2.1). This removed almost all error near the center of force, but did not correct the problems in the step system. It is, therefore, incorrect to use the dipole fields measured asymptotically to compute the displacements of atoms very near the step edge. The results in Fig. 3(a) are probably the best a dipole field can do at predicting displacements near the step edge. This is because the simple surface stress force distribution produces only negligible quadrupole moments. While the quadrupole and higher moments are not defined because of the divergence of the moments, effective higher-order moments exist and are useful if the region of integration in (2.4) is restricted to some L. The difference between the annealed and calculated displacement fields in Fig. 3 is actually the result of octupole terms and higher. In a real crystal, the step edge tries to recoordinate its empty bonds and relaxes into the bulk. This will generate quadrupole moments that will be longer ranged and possibly stronger than the octupole moment generating the error in our simulation. Also, it is clear that the simple continuation of the displacement field into the step system does a poor job reproducing the displacements and that this has nothing to do with the multipole approximation. A correct treatment would use the displacements in the AB plane to compute the displacements in the step system. Note that the atom at the step edge undergoes a much larger displacement than predicted by the simple extension of the displacement field into the step system. This anomalous displacement is also observed in more microscopic treatments.[11] The simple computational treatment above shows that at least in part this is due to the mechanics of the stepped system itself and, therefore, any treatment that tries to model the effect using a force distribution on a flat interface is incomplete.

The simulation clearly shows that the isotropic fields in the previous section are correct, that the dipole fields are the only surviving fields a few lattice spacings from the step edge and that the z-dipole moment is correctly given by ag.

V. CUBIC SYSTEMS

In the next section, experiments that measure the displacement field of a step on Si(111)(7×7) are presented. The isotropic results will be used to analyze the experimental images. Silicon is, however, an anisotropic material. The use of the isotropic displacement fields represents a major approximation and in this section, that approximation is examined. Thus far, we have been unable to find a closed form solution to the full cubic surface line force displacement field. The stress tensor for a line z directed monopole has been calculated by Lekhnitskii.[12] The full solution for the anisotropic stress tensor is so complicated that integration to produce the displacement field is not feasible. There is also a broad literature on the bulk point force problem[13] in the context of dislocation theory.[14] Unfortunately, the solutions to the cubic problem for bulk dislocations are not easily extensible to a surface force distribution because they contain stresses normal to the surface. To evaluate the severity of the isotropic approximation, the mass and spring model of the previous section is used to compare the annealed field of a cubic crystal with the corresponding computed field using the isotropic displacement fields.

The elastic constants for Si at room temperature are: $C_{11}=166$ GPa, $C_{12}=64$ GPa, and $C_{44}=79$ GPa. The effective Lamé coefficients are estimated by using the Voigt average of the stiffness tensor, giving $\mu=C_{44}-H/5$ and $\lambda=C_{12}-H/5$, where $H=2C_{44}+C_{12}-C_{11}$ measures the anisotropy. If $H=0$ then the material is isotropic. For Si, $\mu=67.8$ GPa, $\lambda=52.8$ GPa, and $H=56$ GPa. A dimensionless measure of the anisotropy is $J\equiv H/C_{11}$ which for Si is 0.34. The two-dimensional quantities entering the displacement fields can be calculated in terms of the Lamé coefficients: $\nu_2=\lambda/(\lambda+2\mu)=0.28$ and $E_2=4\mu(\lambda+\mu)/(\lambda+2\mu)=1.08$ eV/Å^3. In the mass and spring model in the previous section, the elastic constants are: $C_{11}=k_1+k_2/2$, $C_{12}=k_2/2$, and $C_{44}=k_2/2$, where k_1 is the spring constant of the springs along the unit cell edges and k_2 is the spring constant of the springs connecting the corners to the mass at the center of the cell. A choice of $k_1=0.62$ and $k_2=1$ results in $H/C_{11}=0.34$ and yields $\nu_2=0.33$ and $E_2=1.13$. With this choice of parameters, the annealed cubic displacement field is compared with the

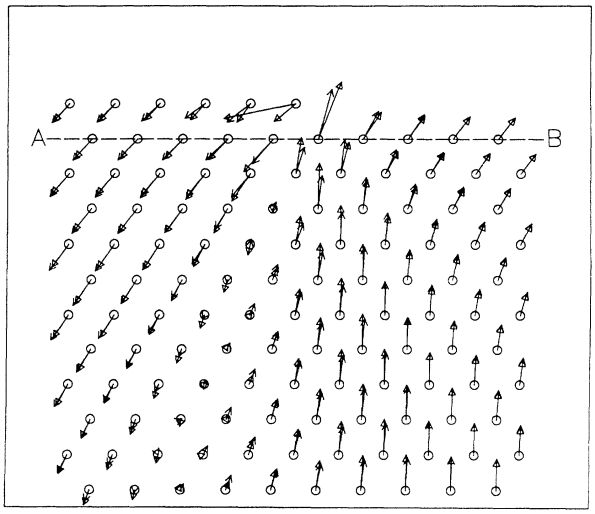

FIG. 4. Computational test of cubic anisotropy. The circles represent the undeformed location of the masses. The open arrowheads are the displacement of the masses upon annealing the cubic crystal multiplied by r and a magnification factor, where r is the distance from the step edge with a cutoff. The closed arrowheads are the calculated isotropic field using only the dipole moments, with the average Poisson's ratio and Young's modulus.

computed isotropic displacement field in Fig. 4. The agreement between the computed and annealed field is still quite good. It is, therefore, satisfactory to use the isotropic displacement fields to extract the dipole moments from a cubic material such as Si. The difference between the isotropic field and the actual cubic displacement field will result in a small error in the measured dipole moment.

VI. EXPERIMENTAL RESULTS

In this section, a TEM image for a monatomic Si(111)(7×7) step is analyzed using the displacement fields computed in (3.4). The leading-order multipole is shown to be the dipole and a value for the dipole moment is extracted from the experimental data.

A. Description of experiment

The technique of dark field imaging in a transmission electron microscope is particularly useful for imaging crystal strain.[15] It involves forming an image with electrons scattered from only one reciprocal lattice plane (e.g., only one Bragg diffracted beam). In a TEM only three types of contrast will be visible at a step: phase contrast, thickness contrast, and strain contrast. Phase contrast arises for the same reason as Fresnel fringes in light optics. An electron's phase depends upon the distance it must travel through a crystal. Since a step is a boundary between regions of differing thickness, the electrons on either side will possess different phases. At the bottom of the crystal, these electrons will interfere to form fringes. For thin samples under near-focus conditions, phase contrast is negligible. Thickness contrast arises from the periodic variation in Bragg beam intensity with depth in the crystal. The period of oscillation depends on the orientation of the crystal with respect to the incident electron beam. Since crystal thickness is quantized, a step will mark a discrete change in the image intensity. This effect can be used to measure the step height. Strain produces lattice plane rotations and thus locally changes the angle of incidence of the electron beam with respect to the reciprocal lattice plane contributing to the image. In this way crystal strain is mapped as changes in intensity in the dark field image.

The full experimental details are given elsewhere.[1] Si(111)(7×7) samples were prepared and placed in a JEOL 200CX TEM modified to provide a UHV specimen environment. Sample areas were characterized by micron-sized flat areas surrounded by highly terraced regions.[16] Typically, the flattest areas were only 300 Å thick. Images were taken using the $\frac{1}{3}\bar{4}22$ and $\bar{2}20$ reflections under a variety of diffraction conditions. The $\bar{2}20$ dark field images revealed the presence of both strain and thickness contrast at steps. Because of the surface sensitivity of $\frac{1}{3}\bar{4}22$ dark field images, it is possible to differentiate between single and triple height steps. Only monatomic steps were chosen for analysis.

Images of monatomic height steps were then digitized for quantitative analysis. Line scans perpendicular to the monatomic steps were performed to measure intensity as a function of distance from the step. One such line scan is shown in Fig. 5 where the step is located at the center of the plot and thickness decreases from left to right. If the step showed only thickness contrast, the intensity profile would be a step function. The oscillations in intensity near the step indicate the presence of strain since the images were taken near focus. The extrema occur roughly 50 Å away from the step and mark where the step strain has rotated the $\bar{2}20$ crystal planes either closest to (maximum) or furthest from (minimum) the exact Bragg condition. This behavior is indicative of a

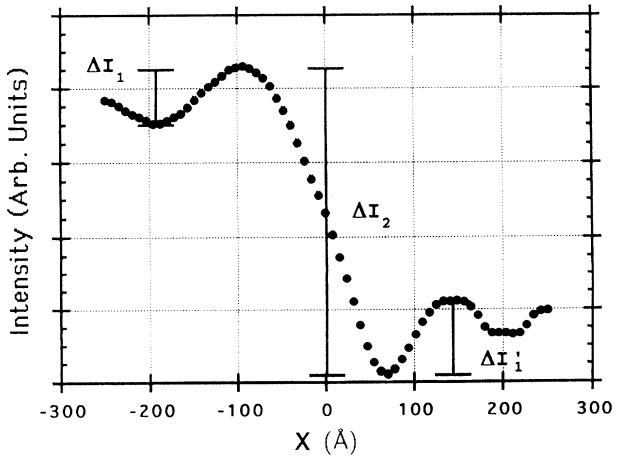

FIG. 5. A line scan from a TEM image showing the intensity pattern for a step on Si(111)(7×7). The step in at $x=0$. The image is a dark field image in the $(g,3g)$ condition where the step normal is parallel g.

change in the sense of lattice plane rotation across the step. Furthermore, unlike phase contrast which would only extend a few angstroms from the step near focus, the contrast in the experimental images persists up to 150 Å away from the step. Images can also be obtained as a function of the deviation parameter. Because of the strong dependence of the experimental contrast on the deviation parameter, one can only conclude that its cause is strain.[15] For Fig. 5, the deviation parameter was measured as 0.010 $Å^{-1}$. It should be noted that during a line scan, the intensity is averaged over two or three pixels where each pixel corresponds to roughly 8 Å. Thus the resolution is only about 20 Å.

Once the experimental images have been digitized, they can be compared with computer simulated images. The method of image simulation involves numerically solving Schrödinger's equation for the illuminating electrons' transit through the crystal and is described in detail elsewhere.[1,17] Strain in the crystal is accommodated using the rigid-ion approximation and it is assumed that the displacement field varies slowly with position. The simulations produce the intensity as a function of position for a stepped surface under the influence of the model strain field. Experimental and simulated images can be compared to determine the order of the leading multipole as the dipole. The magnitude of the x-dipole moment can then be extracted.

B. Qualitative results

The elastic multipole expansion divides the asymptotic displacement fields into universality classes. The asymptotic displacement fields for two systems with the same leading multipole can be collapsed onto a universal curve for that multipole by adjusting $\mathbf{d}^n/E_2$ and ν_2. It is, therefore, possible to determine the order of the leading multipole by comparing the shape of the experimental intensity curve with the shapes of computationally simulated images of various pure multipole fields. In Fig. 6, the simulated images of dipole and monopole fields are presented. The monopole curves are qualitatively different from the dipole curves. The general shape of the simulated intensity plots can be compared with the experimental image of a monatomic step on the (7×7) reconstructed (111) surface of Si,[1] shown in Fig. 5. The x-dipole curve in Figs. 6(a) is the best match for the general shape of the experimental intensity curve. This experimentally establishes the dipole as the leading-order multipole of a step. The z dipole is a minor effect and is added to the x dipole to adjust the asymmetry in depth of the troughs measured by $\Delta I_1 - \Delta I_1'$ in Fig. 5. A qualitative comparison of the simulated intensity curves in Figs. 6(a) and 6(b) with the experimental curve in Fig. 5, leads one to expect the x dipole is the dominant term with a small z-dipole moment. The analysis of the next section bears this out.

C. Quantitative results

To extract the x-dipole moment from the experimental intensity curve, images are simulated for various x-dipole moments using the diffraction condition and thickness (measured for convergent beam electron diffraction) corresponding to the experimental image in Fig. 5. The experimental and simulated images are compared using two statistics which were found to be sensitive to the dipole moments: the step contrast defined as $\Delta I_1/\Delta I_2$ and the asymmetry defined as $\Delta I_1/\Delta I_1'$ as shown in Fig. 5. The simulations use the isotropic dipole fields in (2.3) and the average elastic constants; $E_2 = 1.08$ eV/Å^3, $\nu_2 = 0.28$. The finite thickness of the sample was corrected for by the addition of an image dipole that removed the normal stresses at the bottom surface of the sample. The z-dipole moment is fixed by the experimental value of the surface stress,[18] $g = 0.186 \pm 0.012$ eV/Å^2, and the step height $a = 3.14$ Å, giving $d_z^1 = ag = 0.58 \pm 0.04$ eV/Å. Comparison of experimental and simulated images using the step contrast statistic yields $d_x^1 = 1.66$ eV/Å. The asymmetry statistic gives a value of the x-dipole moment as $d_x^1 = 1.25$ eV/Å. We report the x-dipole moment of a monatomic step on Si(111)(7×7) as $d_x^1 = 1.46 \pm 0.3$ eV/Å, the average of these values. These two statistics have different sensitivities to the components of the dipole moment and to the possible sources of error in the experimental image. The step contrast is dominated by the x-dipole moment

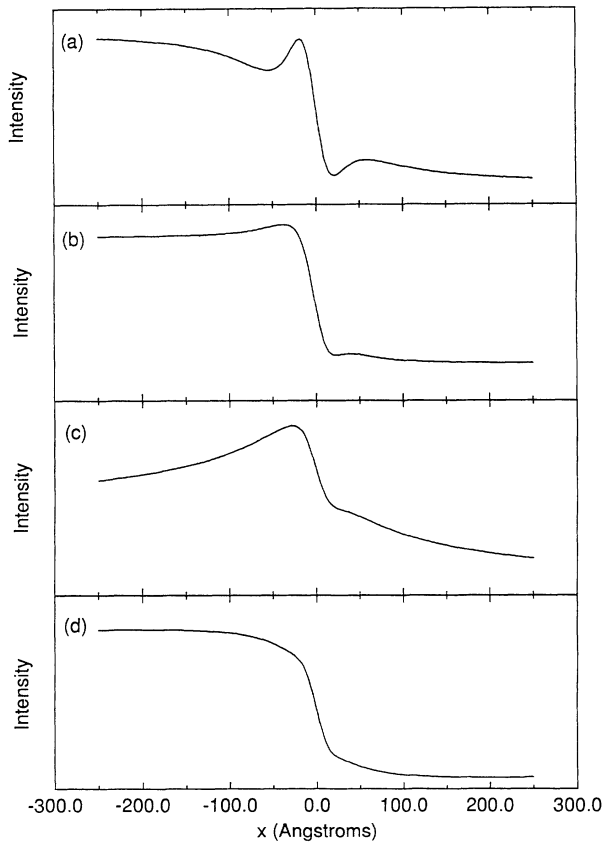

FIG. 6. Simulated intensity plots of low-order elastic multipoles: (a) Pure x dipole field, $\mathbf{d}^0 = 0$, $\mathbf{d}^1 = (1.0, 0.0)$ eV/Å, (b) pure z-dipole field $\mathbf{d}^0 = 0$, $\mathbf{d}^1 = (0.0, 1.0)$ eV/Å, (c) x monopole, $\mathbf{d}^0 = (0.05, 0)$ eV/Å^2, $\mathbf{d}^1 = 0$, (d) z monopole, $\mathbf{d}^0 = (0, -0.05)$ eV/Å^2, $\mathbf{d}^1 = 0$. Images simulated using average Young's modulus and Poisson's ratio for Si and passed through a 30-Å filter.

as can be seen in Fig. 6(a) and is relatively insensitive to the z-dipole moment. Unfortunately, the step contrast is also sensitive to stray monopole moments coming from a slight curvature of the step and sharp surface features far from the step. The asymmetry statistic is controlled by the ratio of the x-dipole moment to the z-dipole moment and should be less sensitive to stray monopoles. The asymmetry, however, is a much smaller effect than the step contrast and, therefore, contains larger statistical errors. Hopefully, the average of these two statistics comes close to capturing the true physical situation. The difference in the two values of the dipole probably indicates a stray monopole field resulting from a slight bending of the step.

When comparing the images simulated with a pure dipolar strain field with those taken from the microscope, differences in the peak position and intensity slope near the step can be seen. This disagreement is not well understood but could derive from a variety of causes. While the experimental intensity profiles were taken from isolated steps, these steps could contain kinks or sharp bends which would introduce a significant monopole term to the strain field. This would tend to shift the intensity extrema further away from the step and decrease the slope at the step. Another complication is the limited experimental resolution. The process of taking an image and then digitizing it tends to smear out abrupt changes in intensity exaggerating the range over which the strain contrast is seen. In the future we hope to be able to use the multipole expansion to analyze the experimental images and extract all the moments. This would allow the monopole effect to be measured and the z dipole to be extracted along with the x dipole.

The data in Fig. 5 were previously analyzed using a model for a stepped surface[1] proposed by Srolovitz and Hirth[19] for relaxations near the step edge. The model used monopole forces at the step to capture the anomalous relaxations of the step edge commented on in Sec. IV. There was some agreement between the simulated images of the monopole model and the experimental data, but qualitative differences were evident. The array of monopoles captured the correct change in sense of lattice plane rotation as the step is crossed, but failed to reproduce the distinctive trough in the experimental image. When an isolated monopole was tried, which was expected to be a better match to the experimental situation, more qualitative problems surfaced in the form of a lack of saturation of contrast changes at infinity. This work resolves the qualitative differences between the simulated images and the experiment, showing that the correct model involves dipole forces.

VII. CONCLUSION

The leading multipole moment of an isolated straight surface step is the dipole moment. The z-dipole moment is fixed by the surface stresses and has the value ag. The x-dipole moment can be fixed by fitting simulated image profiles to image profiles observed in TEM experiments. For Si(111)(7×7), the x-dipole moment is measured as $d_x^1 = 1.46 \pm 0.3$ eV/Å and the z-dipole moment is computed to be $d_z^1 = 0.58 \pm 0.04$ eV/Å.

ACKNOWLEDGMENTS

We acknowledge helpful discussions with R. Tweston, N. Goldenfeld, G. Ehrlich, D. Carlson, A. Howie, L. M. Brown, and D. Srolovitz. J.S. was supported in part by the National Science Foundation through Grant No. NSF-DMR-90-15791. O.P. and J.G. were supported through DOE Grant No. DEFG02-91ER45439. One of us (J.S.) gratefully acknowledges the support of AT&T Bell Laboratories.

APPENDIX

1. Stress and strain tensors of a surface dipole

In this section, the stress and strain fields for a pure dipole are presented. For a pure dipole force, the strain tensor e_{ij} can be written as

$$e_{ij} = M^1_{ijk} d^1_k \ , \tag{A1}$$

where repeated indices are summed and M^1 are defined as

$$\begin{aligned} M^1_{xxk} &= \frac{\partial D^1_{xk}}{\partial x}, \quad M^1_{xzk} = \frac{1}{2}\left[\frac{\partial D^1_{zk}}{\partial x} + \frac{\partial D^1_{xk}}{\partial z}\right], \\ M^1_{zxk} &= M^1_{xzk}, \quad M^1_{zzk} = \frac{\partial D^1_{zk}}{\partial z} \ . \end{aligned} \tag{A2}$$

Differentiating D gives the expressions for the six components of M^1 as

$$\begin{aligned} M^1_{xxx} &= -\frac{2}{\pi E_2 r^6}[x^2(x^2-3z^2)+\nu_2 z^2(z^2-3x^2)] \ , \\ M^1_{xzx} &= -\frac{4xz}{\pi E_2 r^6}(1+\nu_2)(x^2-z^2) \ , \\ M^1_{zzx} &= -\frac{2}{\pi E_2 r^6}[z^2(3x^2-z^2)-\nu_2 x^2(x^2-3z^2)] \ , \\ M^1_{xxz} &= -\frac{4}{\pi E_2 r^6}[-xz(z^2-x^2)-2\nu_2 z^3 x] \ , \\ M^1_{xzz} &= \frac{2(1+\nu_2)}{\pi E_2 r^6} z^2(z^2-3x^2) \ , \\ M^1_{zzz} &= -\frac{4}{\pi E_2 r^6}[-\nu_2 x^3 z + (2+\nu_2) x z^3] \ . \end{aligned} \tag{A3}$$

The strain tensor is related to the stress tensor σ_{ij} by the isotropic constitutive relations:

$$\sigma_{ij} = 2\mu e_{ij} + \lambda \delta_{ij} e_{nn} \ , \tag{A4}$$

where δ is the Kronecker delta and μ and λ are the Lamé coefficients. The Lamé coefficients are written in terms of E_2 and ν_2 as: $\lambda = \nu_2 E_2/(1-\nu_2^2)$ and $2\mu = E_2/(1+\nu_2)$. The stress tensor can also be expressed in the form of (A2):

$$\sigma_{ij} = N^1_{ijk} d^1_k \ . \tag{A5}$$

Substituting M into the constitutive relations gives N^1 as

$$N^1_{xxx}=\frac{2x^2}{\pi r^6}(3z^2-x^2),\quad N^1_{xzx}=\frac{4xz}{\pi r^6}(z^2-x^2)\ ,$$
$$N^1_{zzx}=\frac{2z^2}{\pi r^6}(z^2-3x^2),\quad N^1_{xxz}=\frac{4xz}{\pi r^6}(z^2-x^2)\ , \tag{A6}$$
$$N^1_{xzz}=\frac{2z^2}{\pi r^6}(z^2-3x^2),\quad N^1_{zzz}=-\frac{8z^3x}{\pi r^6}\ .$$

There is also a component of the stress along the step given by $\sigma_{yy}=\nu(\sigma_{xx}+\sigma_{zz})$. Later it will be convenient to examine the stress in cylindrical coordinates where N has the form

$$N^1_{rrx}=\frac{2\cos(2\theta)}{\pi r^2},\quad N^1_{r\theta x}=\frac{\sin(2\theta)}{\pi r^2}\ ,$$
$$N^1_{rrz}=\frac{2\sin(2\theta)}{\pi r^2},\quad N^1_{r\theta z}=-\frac{2\cos^2(\theta)}{\pi r^2}\ , \tag{A7}$$
$$N^1_{\theta\theta x}=N^1_{\theta\theta z}=0\ ,$$

with θ is measured from the $-z$ axis.

2. Displacement field of a stepped surface

The experiment presented earlier was best described by an isolated surface step. A more common geometry is the uniformly stepped surface with an infinite array of steps each separated by a distance Δ. In this section, the calculation of the displacement field of an isolated step is extended to the displacement field of a stepped surface. First, the effect of rotating the separation plane AB is examined and then the displacement field is computed.

Before a displacement field can be computed, a new separation plane must be selected and the dipole moments recomputed. The plane AB is not appropriate for a uniformly stepped surface because it intersects the surface. Clearly, a separation plane parallel to the surface must be chosen. Figure 7 shows the old separation plane AB and the separation plane for a stepped surface CD. Examination of the stress fields (A7) shows that the solution to the surface problem of an isolated step cannot be simply extended to a stepped surface, since the isolated step solution has stress normal to the surface for any separation plane except AB. This is not surprising, because the choice of a separation plane causes a one-dimensional projection of the actual two-dimensional force distribution. There is no reason the result of projecting the force on the plane CD should be simply related to projecting the force on the plane AB. The torque computation in Sec. II can be repeated for the stepped surface using the plane AB as the separation plane. This time the torque from the edges of the crystal about a point in the plane AB directly below the left edge of the crystal is $n_s ag\hat{\mathbf{y}}$, where n_s is the number of steps. Since the surface communicates no net force to the crystal, this is also the moment about any point in the crystal. The force generating this torque is localized at the surface, so if the crystal is separated at the plane CD, a torque $n_s ag\hat{\mathbf{y}}$ is communicated to the bulk crystal through the plane CD. The isolated step result is, therefore, recovered, each step has a z-dipole moment of ag, exactly. This argument leaves the value of the x-dipole moment for the force distribution on the plane CD arbitrary. However, since the magnitude of the displacement field of a stepped surface should be approximately the same as that of an isolated step near the step, it is probably useful to approximate the stepped surface x dipole by the isolated step value. It is important to appreciate the difference in the x- and z-dipole moment results: using the isolated step z-dipole moment for the stepped surface is an exact result of mechanics, using the isolated step x-dipole moment for the stepped surface dipole moment is an uncontrolled approximation based on intuition.

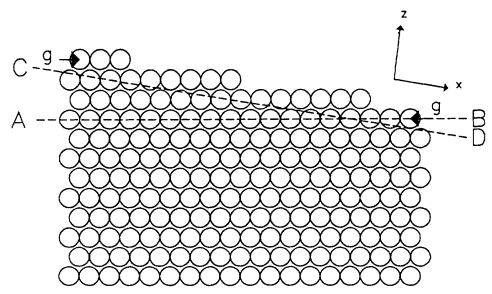

FIG. 7. Two-dimensional crystal with a stepped surface.

The pure dipole displacement field of an isolated step with dipole moments computed along the CD plane in Fig. 7, can be written as $u_i=D^1_{ij}d^1_j$, where the x axis is parallel to CD and the z axis is the outward normal to CD. To compute the displacement field of a uniformly stepped surface, the contributions of each step are added

$$u^s_i(x,z)=\sum_{n=-\infty}^{\infty} D^1_{ij}(x+n\Delta,z)d^1_j\ , \tag{A8}$$

where u^s is the displacement field of the stepped surface and Δ is the step separation. Introducing the stepped dipole fields D^{1s} allows (A8) to be rewritten as $u^s_i(x,z)=D^{1s}_{ij}(x,z)d^1_j$, where

$$D^{1s}_{ij}(x,z)=\sum_{n=-\infty}^{\infty} D^1_{ij}(x+n\Delta,z)\ . \tag{A9}$$

The summation only alters the variable x in the expression for D^1. Examination of (3.4) finds that x only occurs in the combination $h_m(x,z)\equiv x^m/r^4$, $m=0$, 1, 2, and 3. If the expressions h_m in the isolated step displacement field are replaced by

$$h^s_m(x,z)\equiv\sum_{n=-\infty}^{\infty} h_m(x+n\Delta,z)=\sum_{n=-\infty}^{\infty}\frac{(x+n\Delta)^m}{[z^2+(x+n\Delta)^2]^2} \tag{A10}$$

the stepped dipole fields are obtained. Carrying out this substitution, the stepped dipole fields are

$$D^{1s}_{xx}=\frac{2}{\pi E_2}[h^s_3(x,z)-\nu_2 z^2 h^s_1(x,z)]\ ,$$
$$D^{1s}_{zx}=\frac{2}{\pi E_2}[-z^3h^s_0(x,z)+\nu_2 z h^s_2(x,z)]\ ,$$
$$D^{1s}_{xz}=\frac{2}{\pi E_2}[z h^s_2(x,z)-\nu_2 z^3 h^s_0(x,z)]\ , \tag{A11}$$
$$D^{1s}_{zz}=\frac{2}{\pi E_2}[h^s_3(x,z)+(2+\nu_2)z^2 h^s_1(x,z)]\ .$$

All that remains is the computation of the sums in (A10). Fortunately, these are familiar from the theory of bulk dislocations.[14] Introduce the following sums:

$$
\begin{aligned}
S_0 &= \sum_{n=-\infty}^{\infty} \frac{x+n\Delta}{[z^2+(x+n\Delta)^2]^2} \\
&= 2\frac{\pi^3}{\Delta^3 Z}\frac{\sinh(Z)\sin(X)}{[\cosh(Z)-\cos(X)]^2}\ , \\
S_1 &= \sum_{n=-\infty}^{\infty} \frac{z^2-(x+n\Delta)^2}{[z^2+(x+n\Delta)^2]^2} \\
&= \frac{2\pi^2}{\Delta^2}\frac{\cosh(Z)\cos(X)-1}{[\cosh(Z)-\cos(X)]^2}\ , \\
S_2 &= \sum_{n=-\infty}^{\infty} \frac{z^2+(x+n\Delta)^2}{[z^2+(x+n\Delta)^2]^2} \\
&= \frac{2\pi^2}{\Delta^2 Z}\frac{\sinh(Z)}{\cosh(Z)-\cos(X)}\ , \\
S_3 &= \sum_{n=-\infty}^{\infty} \frac{z^2(x+n\Delta)+(x+n\Delta)^3}{[z^2+(x+n\Delta)^2]^2} \\
&= \frac{\pi}{\Delta}\frac{\sin(X)}{\cosh(Z)-\cos(X)}\ ,
\end{aligned}
\tag{A12}
$$

where $X=2\pi x/\Delta$ and $Z=2\pi z/\Delta$. The functions h^s are easily expressed in terms of S giving

$$
\begin{aligned}
h_0^s &= \left[\frac{2\pi^2}{\Delta^2}\right]\frac{S_1+S_2}{Z^2},\quad h_1^s=S_0\ , \\
h_2^s &= \frac{S_2-S_1}{2},\quad h_3^s=S_3-\left[\frac{\Delta}{2\pi}\right]^2 Z^2 S_0\ .
\end{aligned}
\tag{A13}
$$

The results from the theory of dislocations were first applied to a stepped surface by Srolovitz and Hirth.[19] The displacement field for a stepped surface obtained by combining (A11), (A12), and (A13) is extremely complicated. Writing it out in full conveys no greater insight than the combination of expressions (A11), (A12), and (A13) above and is not presented. It is more instructive to examine the field in the interesting $z\to 0$ and $z\to-\infty$ limits. First examine how the surface disturbance decays into the bulk by setting $X=0$ and taking the $z\to-\infty$ limit which yields $D^{1s\infty}$:

$$
\begin{aligned}
&D_{xx}^{1s\infty}=0,\quad D_{zx}^{1s\infty}=-\frac{1-\nu_2}{E_2\Delta}\coth\left[\frac{Z}{2}\right], \\
&D_{xz}^{1s\infty}=\frac{1-\nu_2}{E_2\Delta}\coth\left[\frac{Z}{2}\right],\quad D_{zz}^{1s\infty}=0\ .
\end{aligned}
\tag{A14}
$$

The disturbance at the surface decays exponentially into the bulk with a characteristic distance of the step spacing. This result was also found for an array of point monopoles[19] and, therefore, should be considered a general property of regular arrays of point forces. It is also interesting to examine the displacement field at the surface, setting $z=0$ yields

$$
\begin{aligned}
&D_{xx}^{1s}(x,0)=\frac{2}{E_2\Delta}\cot\left[\frac{X}{2}\right],\quad D_{zx}^{1s}(x,0)=0\ , \\
&D_{xz}^{1s}(x,0)=0,\quad D_{zz}^{1s}(x,0)=\frac{2}{E_2\Delta}\cot\left[\frac{X}{2}\right].
\end{aligned}
\tag{A15}
$$

In future work, this expression will be used to compute the surface free energy due to elastic interactions of a stepped surface.

[1] O. Pohland, X. Tong, and J. M. Gibson, J. Vac. Sci. Technol. A **11**, 1837 (1993).

[2] H. Sato and K. Yagi, J. Phys. Condens. Matter **5**, 2095 (1993).

[3] Hans-Werner Fink and Gert Ehrlich, Surf. Sci. **143**, 125 (1984).

[4] S. C. Wang and Gert Ehrlich, Phys. Rev. Lett. **70**, 41 (1993).

[5] K. H. Lau and W. Kohn, Surf. Sci. **65**, 607 (1977).

[6] F. Wantanabe and G. Ehrlich, J. Chem. Phys. **96**, 3191 (1992).

[7] J. M. Rickman and D. J. Srolovitz, Surf. Sci. **284**, 221 (1993).

[8] V. I. Marchenko and A. Ya. Parshin, Zh. Eksp. Teor. Fiz. **79**, 257 (1980) [Sov. Phys. JETP **52**, 129 (1980)].

[9] P. Nozières, in *Solids Far from Equilibrium*, edited by C. Godrèche (Cambridge University Press, Cambridge, 1992).

[10] A. E. H. Love, *A Treatise on the Mathematical Theory of Elasticity*, 4th ed. (Dover, New York, 1944); Adel S. Saada, *Elasticity: Theory and Applications* (Pergamon, New York, 1974).

[11] S. P. Chen, A. F. Voter, and D. J. Srolovitz, Phys. Rev. Lett. **57**, 1308 (1986).

[12] S. G. Lekhnitskii, *Theory of Elasticity of an Anisotropic Elastic Body* (Holden-Day, San Francisco, 1963).

[13] Early work includes I. M. Lifshitz and L. N. Rozentsveĭg, Zh. Eksp. Teor. Fiz. **17**, 783 (1947); J. D. Eshelby, W. T. Read, and W. Shockley, Acta Metall. **1**, 251 (1953).

[14] J. P. Hirth and J. Lothe, *Theory of Dislocations*, 2nd ed. (Wiley, New York, 1982), p. 732.

[15] P. Hirsch, A. Howie, R. Nicholson, D. W. Pashley, and M. J. Whelan, *Electron Microscopy of Thin Crystals* (Krieger, Malabar, FL, 1977).

[16] J. M. Gibson, *Surface and Interface Characterization by Electron Optical Methods* (Plenum, New York, 1988), p. 55.

[17] A. Howie and Z. S. Basinski, Philos. Mag. **17**, 1039 (1968).

[18] R. E. Martinez, W. M. Augustyniak, and J. A. Golovchenko, Phys. Rev. Lett. **64**, 1035 (1990). The experiment measures the stress difference between Si(111)(7×7) and a reference surface and then computes the stress in Si by using a theoretical value for the stress on the reference surface.

[19] D. J. Srolovitz and J. P. Hirth, Surf. Sci. **255**, 111 (1991).